Phys. Status Solidi C **14,** No. 3-4, 1700034 (2017) / **DOI** 10.1002/pssc.201700034

physica status solidi c
www.pss-c.com
current topics in solid state physics

A space-charge-free CdS, and a new solar cell without *pn*-junction enabled by high-field domains

Karl W. Böer*,**

Retired, Department of Physics and Astronomy, University of Delaware, Newark, DE, USA

Received 26 January 2017, accepted 26 January 2017
Published online 20 March 2017

Keywords electrode-adjacent domains, hole injection from Au, life equation, minimum entropy production principle, new solar cell model without a *pn*-junction, *p*-type CdS, precise spreading of quasi-Fermi levels, sharp quenching signal in pure CdS, space-charge-free crystal, work function development

* Corresponding author: e-mail karlwboer@gmail.com, Phone: +1 239 261 2424, Fax: +1 239 530 2424
** Present address: 138 Moorings Park Drive, Naples, FL 34105, USA

A review of the electrical properties of a copper doped CdS as a model semiconductor describing three independent thermodynamic states depending on optical excitation and bias. These are the traditional ground state that, dependent of optical excitation renders it from an insulator to a highly conductive *n*-type semiconductor. With higher applied voltage, a high-field domain occurs that is locked-in, attached to the cathode. It presents the second thermodynamic stable state that is *n*-type with constant drift current limited by the carrier density at a blocking electrode n_c. With further increased bias, the high-field domain becomes anode-adjacent. The CdS is in its third thermodynamic stable state. Here, the CdS has flipped into *p*-type conductivity with the current limited by the hole density at the blocking anode p_a. In both states, the CdS is free of space charges within the domain that permits defect level spectroscopy without broadening influence of fluctuating electric fields. The minimum entropy production principle connects the work functions of blocking cathode and anode by the constant domain current, and permits the measurement of their values that depend on the optical excitation. A new solar cell is described that works without a *pn*-junction, with a thin, pure CdS layer replacing the junction. The CdS extracts the holes for tunneling into the base electrode. The CdS/CdTe to scale model is given as an example. It has substantial increased efficiency by preventing junction leakage and permits an increase of the open circuit voltage to approach the theoretical limit of the band gap of the emitter when extrapolated to 0 K. The solar cell is series resistance limited by the CdS and requires a thin planar deposition of CdS. Since CdS is photoelectrically passive, its Fermi-level at the base electrode is fixed. A Gallium doping of a thin layer pins the Fermi level within 0.05 V to the conduction band and increases V_{oc} further. All properties of CdS with high-field domains are described quantitatively and the domains are made visible by the Franz–Keldysh effect.

1 Electrical properties of CdS in the ground state

1.1 Introduction The electrical properties of CdS in its ground state are briefly reviewed. In the second part, the electrical properties of CdS are discussed when high-field domains are present. This part is divided into two sections of different thermodynamic stable high-field electrical states of CdS, one, when the domain is attached to the cathode and the CdS is *n*-type, and the other one when the domain is attached to the anode and the entire CdS has turned *p*-type.

1.1.1 Current–voltage characteristics The current as a function of the applied voltage is the primary tool to investigate the electrical properties. Attention is given to its deviation from ohmicity. Two examples are given for the model semiconductor [1] CdS in Figs. 1 and 2.

Without doping, the voltage can be varied over a wide range when a series resistance prevents a premature dielectric breakdown. Figure 1 shows the characteristic with the light intensity as family parameter. At higher light intensities non-ohmicity is observed with negative differential conductivities due to field quenching of Coulomb attractive hole traps. At lower light intensities, the range of ohmicity can be extended. At a critical value (here, 0.25 W), current channels form and *thermal breakdown* follows for the unprotected crystal.

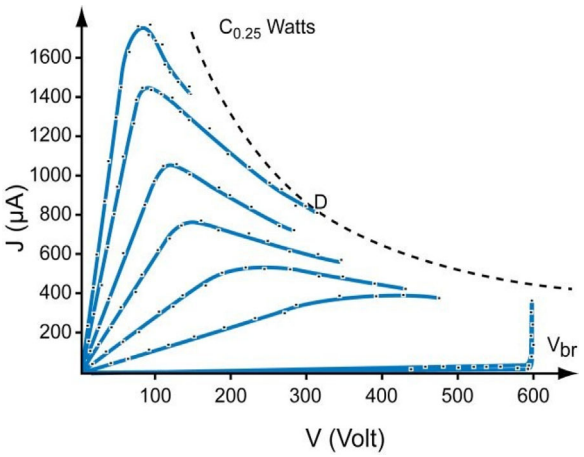

Figure 1 *j-V* characteristics for CdS with light intensity as family parameter, showing some field quenching [4]. Reproduced with permission from Annalen der Physik, 527.5-6, 378 (2015). Copyright 2015, John Wiley and Sons.

In Fig. 2, at lower light intensities the current remains ohmic up to the breakdown threshold. With further increase in optical excitation, the current becomes over-ohmic indicating field excitation from electron traps. At a critical voltage, field ionization starts with a steep increase in current that leads to the *dielectric breakdown* of the unprotected crystal.

2 Electrical properties with high-field domains

For all following experiments, the electrode geometry given in Fig. 3 is used, to permit looking through the crystal between the electrodes in monochromatic light near the absorption edge to visually observe the field distribution using the Franz–Keldysh effect.

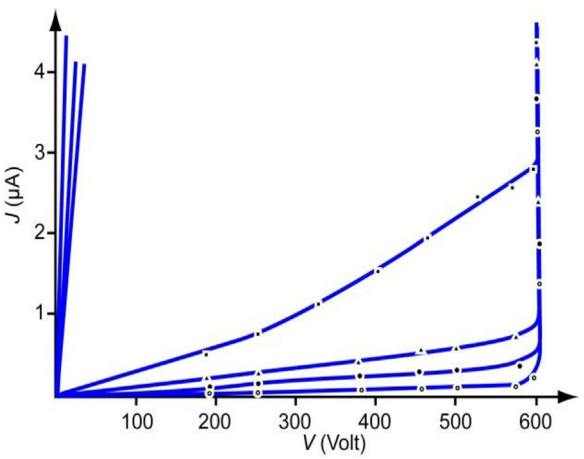

Figure 2 Same as Fig. 1, but for lower light intensities showing slight electron excitation from traps at the higher intensity with an upward bending [2]. Reproduced with permission from Annalen der Physik, 527.5-6, 378 (2015). Copyright 2015, John Wiley and Sons.

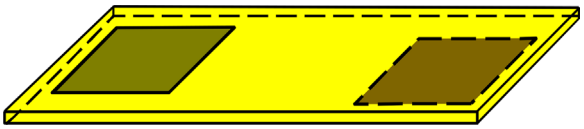

Figure 3 Typical arrangement of the slit electrodes on opposite sides of the CdS crystal to avoid glide discharges [2]. Reproduced with permission from Physica Status Solidi (b), 4, 237 (1964). Copyright 2006, John Wiley and Sons.

2.1 Electroptical search for field inhomogeneities

The first high field domains observed in April, 1958 formed a ring surrounding the cathode.

2.1.1 First experimental observations of high-field domains The first photo of a high-field domain using the Franz–Keldysh effect is shown in Fig. 4, in a CdS crystal platelet with small circular evaporated gold electrodes at dry ice temperatures. With increased applied voltage, *ring-like darkening* appears and, in time, the ring increases in diameter. When the ring touches the anode, it disappears and a new ring emerges from the cathode [3, 4]. The process is reproducible over many days.

With the moving rings, the current oscillates. It is lowest when the ring is in the crystal and increases steeply when the ring disappears.

This phenomenon started a new field in semiconductor physics, the *visual observation of field inhomogeneities in CdS single crystal platelets*.

3 Stationary high-field domains

These domains have created a large theoretical and technical interest.

3.1 The Schöll and Böer domains

When the high-field domains detach themselves from the electrodes, they move and make themselves known by current oscillations as discovered in our laboratory in 1958 [5]. At the March meeting of the German Physical Society in 2011, the name, Böer domain, was given for these domains (Klaus Thiessen introduced this term at the Semiconductor Session of the March Meeting of the German Physical Society in 2001, and it was accepted by all present [6]). But, Ekkehard Schöll explained the moving domains or fluctuations correctly first and prompted the publication of hundreds of publications and dozens of books [7]. We are proposing the name Schöll domain for all moving domains and fluctuations. We restrict the name Böer domain solely for *stationary domains* that attach to electrodes or junctions.

3.2 Cathode-adjacent high-field domain, the Böer domain

When the applied voltage is high enough to initiate significant field quenching, the current decreases with increasing bias. When the quenching increases stronger than linearly with the electric field, a high-field domain *must be created* [8]. Here a band with the lower conductivity is introduced between the electrodes to keep the current lower. This is caused by the strong minimum entropy law. With

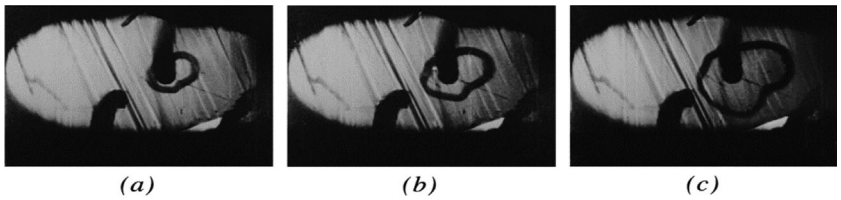

Figure 4 Sequence of photographs, 10 s apart taken by Ulrich Kümmel, of a CdS crystal platelet with circular small gold electrodes, taken near the optical absorption edge at −70° C with 200 V applied [3]. Reproduced with permission from Zeitschrift für Physik, 155.2, 170 (1959). Copyright 1959, Springer.

increased bias the current no longer increases but the domain width increases to absorb the increased bias.

3.3 The field-of-direction analysis The criterion for such domain to appear follows from an analysis of the solution curves of the system of transport and Poisson equation [9] that in its simplest one-dimensional form for electrons reads (the transport Eq. (2) is rewritten to show both as a system of differential Eqs. (3 and 4)):

$$j = en\mu F + \mu kT\frac{dn}{dx}, \tag{1}$$

$$\frac{dn}{dx} = \frac{1}{\mu kT}(e\mu nF - j), \tag{2}$$

$$\frac{dF}{dx} = \frac{e}{e_0 e_{st}}\rho(x), \tag{3}$$

with n the electron density, μ the mobility, F the electric field, j the current density, E_{st} the static dielectric constant, and E_0 the permittivity of space. $\rho(x)$ is the space charge density which contains the reaction kinetic excitation, trapping, and recombination processes as shown in Fig. 5. These transitions are extensively analyzed using kinetic experiments and are well-known for photoconductive CdS [10–13]. The copper-induced hole trap is Coulomb attractive and has the largest cross section for hole trapping. It stores most of the optically excited holes to maintain a large photoconductivity. These centers can be depleted (Fig. 5b) by the electric field.

The Coulomb attractive copper center can be easily ionized by Frenkel–Poole excitation. At low fields the holes are excited into the valance band (Fig. 5) with δE the lowering of the barrier and Z the charge of the Coulomb-attractive center [14]:

$$\delta E = e\frac{eFZ}{\pi e_{st} e_0}, \tag{4}$$

causing "field quenching." This excitation becomes important when $\delta E = kT$, or at about 10 kV cm^{-1}, that is at much lower fields than other field excitation mechanisms such as impact or tunnel ionization.

For the discussion of the solution curves of Eqs.(2 and 3), we deviate from the classical approach of using numerical integration, and use a graphic analysis: In a two-dimensional rendering by projecting any solution curves $n(x)$ and $F(x)$ into an arbitrary nF-plane, the field-of-directions [15] discussion of solution curves becomes more precise: Each point of any solution is uniquely characterized by a point with an angle as shown by short arrows in Fig. 6. With the help of two auxiliary functions we can bring order into this field: the neutrality curve, $n_1(F)$ at which $dF/dx \equiv 0$, and the drift current curve $n_2(F)$, at which $dn/dx \equiv 0$. With these auxiliary curves, the nF-plane can be divided into the four quadrants of directions (Fig. 6). In the first quadrant (I), the direction points to the right and down ($dn/dx < 0$, $dF/dx > 0$), in the second quadrant (II), the direction points right and up ($dn/dx > 0$, $dF/dx > 0$), in the third quadrant (III), the direction points left and up ($dn/dx < 0$, $dF/dx > 0$) and in the fourth quadrant (IV), both directions point down ($dn/dx < 0$, $dF/dx < 0$). Hence, the neutrality curve can only be crossed vertically, and the drift current curve can only be crossed horizontally. Any stationary solution in a finite crystal must end at the singular point where $dn/dx = dF/dx = 0$. Hence, the only stationary solutions must start from an injecting contact in quadrant I or from a blocking contact in quadrant III.

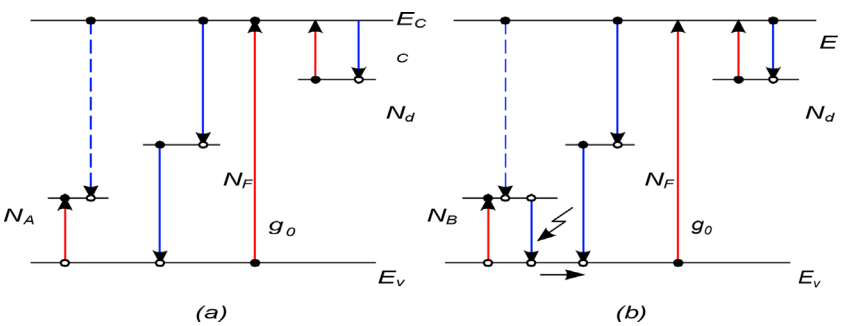

Figure 5 Band model of photosensitized CdS (a) with sensitizing (Cu) centers (N_A) with low recombination (b) With an electric field the holes from these sensitizing centers are freed and can be captured by recombination centers N_F to increase the recombination. g_0 is the optical excitation rate [2]. Reproduced with permission from Physica Status Solidi (b), 39.2, 391 (1970). Copyright 2006, John Wiley and Sons.

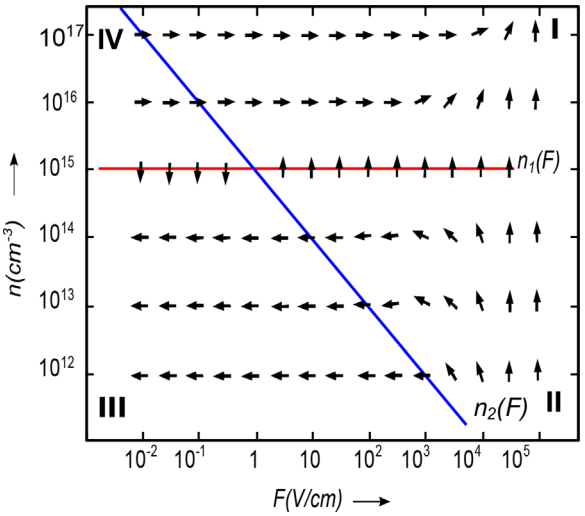

Figure 6 Field-of-direction with $n_1(F)$ the neutrality electron density with $n = \text{const.}$, and $n_2(F)$ the drift current curve with $nF = \text{const.}$ The crossing of both curves shows the singular point where both n and F are constant [15]. Reproduced with permission from Physical Review B, 13.12, 5373 (1976). Copyright 1976, American Physical Society.

3.4 The Schottky barrier Using the field-of-direction approach, we analyze as example the Schottky barrier: starting at a given boundary condition, for instance, at $n_c < n_1$ for a blocking electrode, the solution curve must follow the angle of direction, as shown in Fig. 7. That is, F_c must be selected precisely, so that the solution arrives at the bulk where $dn/dx = dF/dx = 0$, that is, at the singular point **I** in Fig. 7, where the electron density and the field are constant [16].

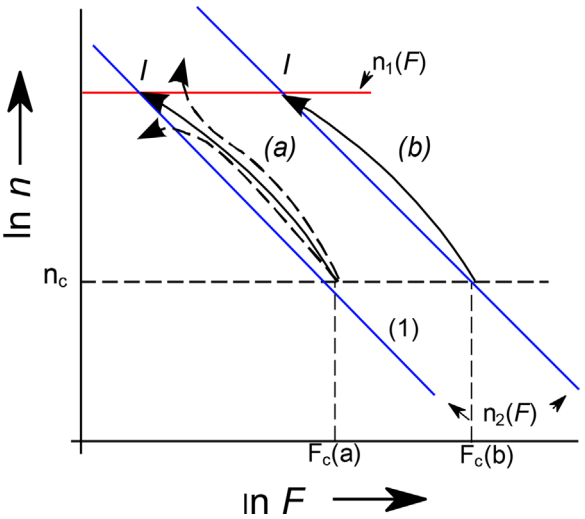

Figure 7 With n_c given at the cathode, the field F_c is uniquely defined in order for the solution to approach asymptotically the constant values of n and F in the bulk, that is at **I**. For initial points that are slightly off from $F_c(a)$, the solution curve misses **I** (dashed curves). At higher applied voltage, the drift current curve is shifted up and to the right, and the new solution (b) is shifted accordingly [15]. Reproduced with permission from Annalen der Physik, 527.5-6, 378 (2015). Copyright 2015, John Wiley and Sons.

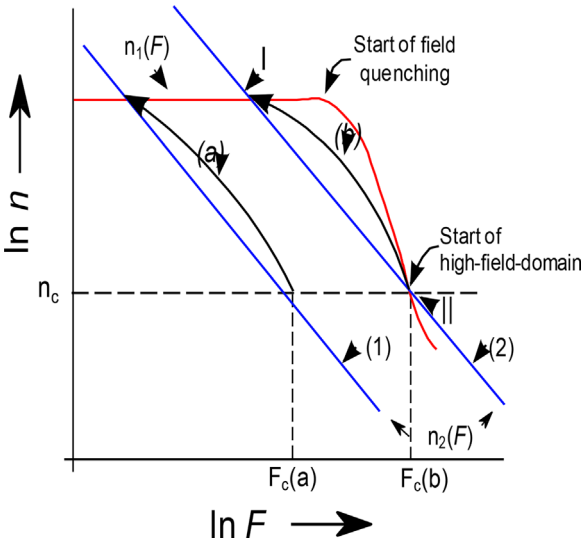

Figure 8 Field-of-direction representation of a typical Schottky barrier solution (a) and of a high-field domain solution (b), the latter occurs when both n_1 and n_2 cross each other at a new singular point **II**, that is determined by n_c. This domain starts at the singular point with a horizontal slope of $n(x)$ and $F(x)$ [15]. Reproduced with permission from AIP Conference Proceedings, 466.1, 3 (1999). Copyright 1999, AIP Publishing LLC.

When at higher fields substantial field quenching occurs, the $n_1(F)$ curve decreases, as shown in Fig. 8. When the decrease becomes over-linear, a **high-field domain** must occur as soon as the drift-current curve $n_2(F)$ crosses $n_1(F)$ again at a given boundary concentration of the blocking contact, n_c.

When the domain is formed, the drift current curve is stuck at **II**, the current saturates. The solution curve extends flat from the junction interface until the excess field is consumed and the field then drops within a few Debye lengths to the bulk until it reaches the anode close to the singular point **I**. At the cathode, the high-field domain starts close to the singular point and the solution curve flattens out: the *Schottky contact has changed into a neutral contact*. This solution is distinctly different from the well-known Schottky barrier, where the electron density declines steeply as it departs from the cathode. Within the domain, the electron density remains initially constant, until, closer to the anode, the field decreases within a few Debye lengths, and then, remains constant again until it reaches the anode. The space charge region is now shifted from the cathode to the end of the domain.

3.5 Direct observation of the Böer domain The cathode-adjacent stationary domains are observed as darker region near the right electrode (Fig. 9). The width of the domain increases with increased applied voltage (a) linearly as shown in (b). From the slope the domain field of 83 kV cm^{-1} is obtained. During the entire operation, the current remains constant near 0.4 mA cm^{-2} as shown

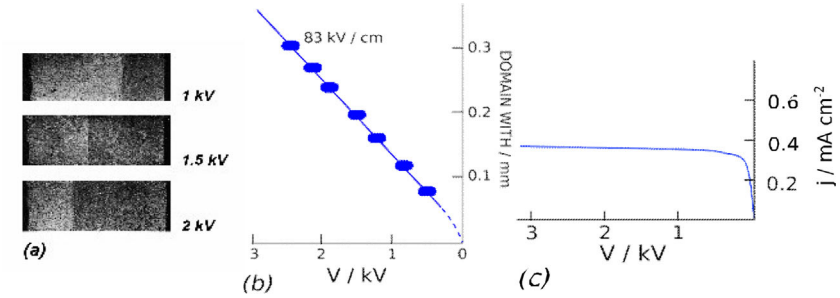

Figure 9 Darkening of part (Franz–Keldysh effect) of a CdS crystal platelet photographed at $\lambda = 540$ Å, at three applied voltages (a). The width of the darkened band (the high-field domain) attached to the cathode at right, increases linearly with bias (b). While the domain is present, the current through the crystal remains constant (c) [2]. Reproduced with permission from Annalen der Physik, 527.5-6, 378 (2015). Copyright 2015, John Wiley and Sons.

in (c), that is caused by the minimum entropy condition that keeps the current at its lowest value.

3.5.1 The second thermodynamically stable conductivity state of CdS The domain is stabilized by the limited electron concentration at the Schottky barrier, n_c: that is, with slight variation in external conditions (bias, temperature, or optical excitation), they return to their thermodynamic stable condition. This indicates that the field-quenched state within the domain is a *second thermodynamically stable state of the conductivity of CdS that is now locked at higher electric fields* [2].

3.6 Anode-adjacent domain at higher fields When extending the neutrality curve in the field-of-direction, field-quenching reaches its maximum value and the $n_1(F)$ curve increases (Fig. 10). This causes a third singular point (III) to occur by intersecting $n_1(F)$ and $n_2(F)$ again [17]. However, now CdS is ambipolar.

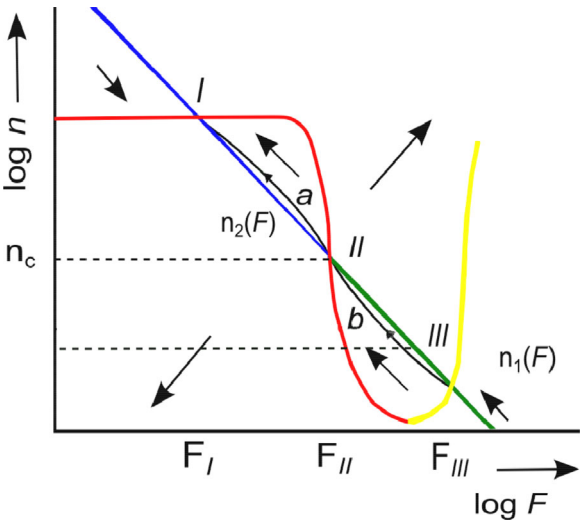

Figure 10 Field-of-direction diagram as in Fig. 8, but now in three dimensions with blue and red for electrons and yellow and green for holes. The diagram is extending to higher fields, exposing another singular point **III** at the third intersection of n_1 and n_2. Curve *a* shown in blue represents the cathode-adjacent, curve *b* shown in green represents the anode-adjacent domain (observe the changing directions of the arrows from *a* to *b*; as we will see in later sections, the crystal here is *p*-type, and the arrow in a two-dimensional discussion in an (*n, p, F*) diagram is beyond the scope of this article, therefore, the note is only here).

3.6.1 The CdS is ambipolar In addition to the electron current, one has now to add the current equations for holes to the set of Eqs. (1)–(3):

$$j_p = ep\mu_p F + \mu_p kT\frac{dp}{dx}, \tag{5}$$

Since drawing a three-dimensional field-of-direction diagram would be confusing, we put on top of each other the two diagrams: $n(F)$ and $p(F)$ but distinguished them in different colors.

3.6.2 Transition between the two types of stationary domains At the transition between cathode and anode adjacent domain, an abrupt change of the direction of the solution is observed: the *anode has flipped* from the singular point **I** to the singular point **III**, with a change in the field-of-direction: the anode-adjacent domain is coming out from the anode and increases in width toward the cathode with increasing applied voltage (Fig. 11). This signalizes that the anode-adjacent domain is a hole domain and the crystal has switched to be *p*-type.

This transition from cathode-to anode-adjacent Böer domains is shown in Fig. 11. The cathode is at the left, the anode at the right, and the electrodes are evaporated at the edges of the CdS. Neglect the crystal striation seen in these pictures (the semicircles are the shadow pictures of the bent electrodes to avoid scratching).

From the slope of the domain width with bias, one obtains $80\,\mathrm{kV\,cm^{-1}}$ for the field in the cathode-adjacent domain, and $135\,\mathrm{kV\,cm^{-1}}$ for the field of the anode-adjacent domain (see Fig. 12a).

During the transition from the cathode-adjacent to the anode-adjacent domain, the current remains saturated without a break in the characteristic, since the minute shift from below to above II is not detectable; the transition point is indicated by an arrow over the characteristic (Fig. 12b).

The anode-adjacent domain is *stabilized* by the limited supply of holes from the hole blocking anode. This is caused by *the thermodynamic principle* to maintain the *state of lowest current through the crystal and the external circuit* (***the minimum entropy principle***). Only when, with increased bias, the anode-adjacent domain fills the entire

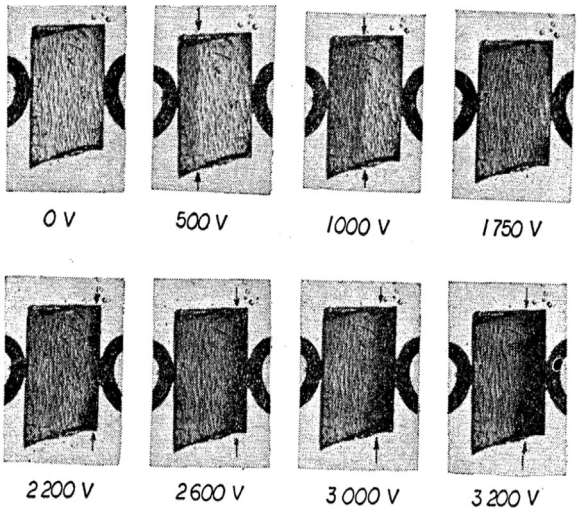

Figure 11 Cathode-adjacent Böer-domain extending from 500 to 1,700 V bias, then filling the entire crystal. When increasing the bias further, a new high-field Böer-domain extends from the anode starting at about 2 kV as shown in the lower row of photos and has substantially higher field as indicated by the increased density of the domain picture [15]. Reproduced with permission from Physical Review, 171.3, 899 (1968). Copyright 1968, American Physical Society.

crystal, can a breakdown occur by field excitation from defects or across the band gap, if not prevented by an external series resistance.

3.6.3 CdS has a third thermodynamically stable state of conductivity As a consequence of these results, we conclude that there are *three thermodynamically stable states of conductivity* in CdS, the normal, low-field case that is conventionally described, and two high-field cases that can be initiated by high-field domains, one which is *n*-type and stabilized by cathode-adjacent domains with limited supply of electrons from the blocking cathode, and one that is *p*-type and stabilized by anode-adjacent domains by the limited supply of holes from the blocking anode.

3.6.4 The evidence that CdS is *p*-type CdS shows a typical quenching spectrum of electrons from traps (Fig. 13) at low fields or when at higher applied voltage a cathode adjacent domain is present. However, with an anode-adjacent domain, the entire crystal has become *p*-type and the quenching spectrum is inverted to an excitation spectrum (Fig. 13).

3.6.5 The band model for cathode- and anode-adjacent domains The band model of the domains is given in Fig. 14a for the cathode-adjacent and in Fig. 14b for the anode-adjacent domain.

Within the domains, the CdS is *space-charge-free* except for the small transition region between both domains where space charges accommodate the changes of the electric fields. Within the domains and adjacent part of the CdS both quasi-Fermi levels are parallel to each and the current is by drift only, except for the transition range between the domain where all current components contribute.

In the high-field domains, the carrier densities, mobilities, and work functions can be determined without ambiguities of the acting fields.

3.6.6 Electron and hole densities as a function of the electric field In the anode adjacent high-field domain the carriers are holes and the current is by drift:

$$j_p = ep\mu_p F. \tag{6}$$

From Eq. (6), one calculates that the hole density is larger in the anode-adjacent than in the cathode adjacent domain by a factor of $(p/n = \mu_n/\mu_p \times (E_{II}/E_{III}) = (300/50) \times (85/125) = 4$. This factor was used for the right side of the scale for holes in Fig. 15. The entire crystal is now in the *third stable conduction state*. Since this state is a partner of the CdS/CdTe solar cell, we will call this in contrast to photoconducting CdS, the third state as the *photovoltaic* CdS state (the application of CdS as a cover layer to make CdTe more efficient solar cell has been pointed out earlier [18], and is recently confirmed by field limitations between 32 and 35 kV cm^{-1} in the CdTe part of the cell [19]).

The entire carrier density distribution of the homogeneous CdS can be obtained through electrode-adjacent domains using various light intensities [20] and is shown in Fig. 15. It is the electron density as function of the field below the minimum shown in red and the hole density above the minimum shown in green.

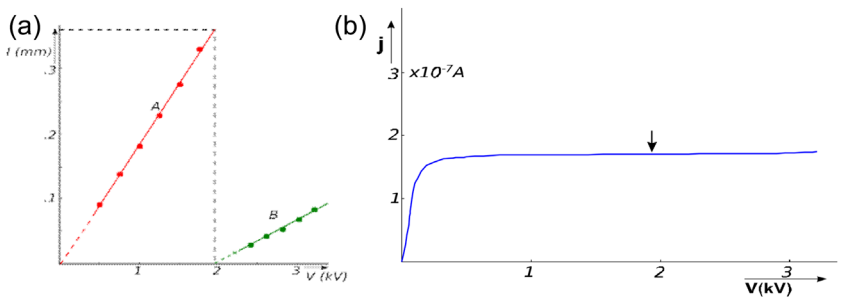

Figure 12 (a) Domain width as a function of the applied voltage for the cathode-adjacent (A) and for the anode-adjacent domain (B). (b) The current–voltage characteristic is taken of the same crystal. During the transition from A to B, the current *remains constant* as shown in the right diagram (b) with the arrow pointing out the transition at about 2 kV. The color changes indicate a change from electron to hole current in A and B (for explanation, see below) [16]. Reproduced with permission from Physical Review, 171.3, 899 (1968). Copyright 1968, American Physical Society.

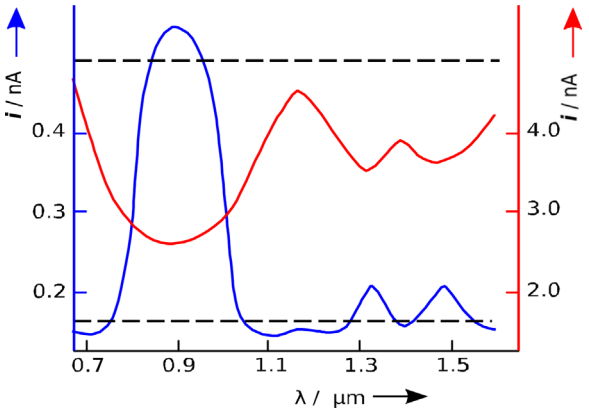

Figure 13 Photocurrent through a CdS single crystal irradiated with a primary beam at 515 mμ as a function of the wavelength of a secondary IR irradiation at low bias showing the typical quenching spectrum of trapped holes, and at high bias when an anode-adjacent Böer domain is present showing infrared excitation with maxima of quenching and excitation coinciding at the well-known hole centers at wavelength 0.9, 1.2, 1.32, and 1.5 μm [15]. Reproduced with permission from Physical Review, 154.3, 757 (1967). Copyright 1967, American Physical Society.

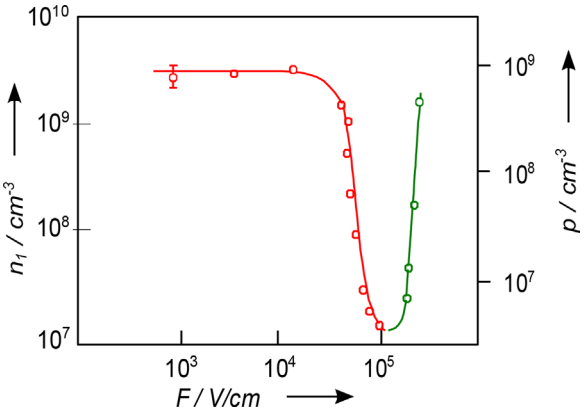

Figure 15 CdS crystal with the cathode adjacent domain below 85 kV cm^{-1} permits to obtain the left branch with the electron density is declining with field. From anode-adjacent domains, above 130 kV cm^{-1}, the right branch of the hole densities is shown and is increasing with field [16]. Reproduced with permission from Physical Review B, 7.4, 1433 (1973). Copyright 1973, American Physical Society.

3.6.7 Determination of the work function as a function of the optical excitation Since electrode-adjacent domains convert a blocking contact into a neutral contact, one can measure sensitive changes of this "effective work function" with the optical excitation of CdS in a wide range of wavelengths.

The domain is pinned by the electron density n_c at the blocking cathode. However, the domain changes with changing optical excitation, causing a parallel shift of the current curve. The work function changes with light intensity. The work function decreases typically by 60 meV with an increase of the light intensity by two orders of magnitude (Fig. 16a) [21]. Different blocking metals show a similar light intensity dependence (Fig. 16b). For every metal, a different CdS crystal (though of similar doping) was used. The similarity of the results given in Fig. 16b, indicate that the light intensity dependence is not drastically influenced by some differences in the defect structure of the CdS [22, 23]. Note: an influence of the space charge region very close to the cathode is however expected; for more details see below.

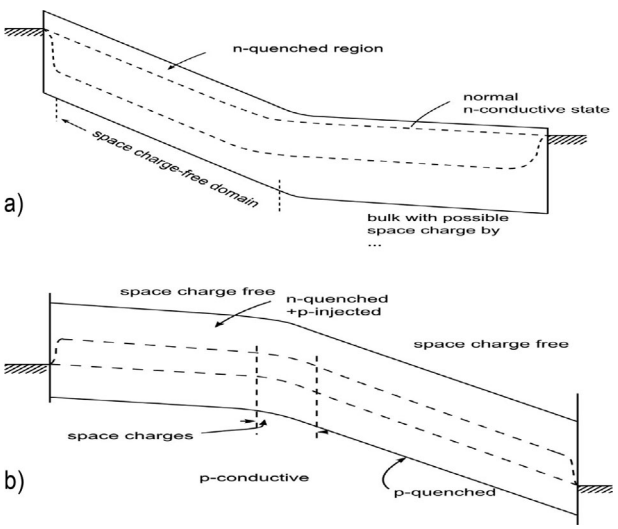

Figure 14 (a) Cathode-adjacent high-field domain, CdS is *n*-type. (b) Anode-adjacent high-field domain CdS has turned *p*-type. Reproduced with permission from Physica Status Solidi (b), 253.8, 1629 (2016). Copyright 2016, John Wiley and Sons.

3.6.8 The spread of the quasi-Fermi levels and the effective work function The electrode-adjacent domains can spread the quasi-Fermi level to a precise value by adjusting the light intensity and then freezing this state while working within the electrode-adjacent high-field domain state. This all can be best explained by looking at this slab starting from a blocking Schottky contact with a developing depletion space charge region and increasing field, until it reaches field were field quenching starts causing a diminishing space charge, until it is completely compensated and the high-field domain starts (Fig. 17).

The thin region between the metal surface and x_c determines the actual work function. This is more defined than in an ordinary crystal at which this potential maximum that defines the critical energy of electrons necessary to escape the metal depends on the doping, that is, on the space charge that increases with applied voltage. That is taken into consideration by the conventional calculus of the characteristics of typical Schottky barriers. With the high-field domain starting, the conditions are precisely defined. We therefore call the resulting measurable work function the *effective work function*.

3.6.9 Small signal lock-in methods Within the high-field domain, the quasi-Fermi levels are precisely

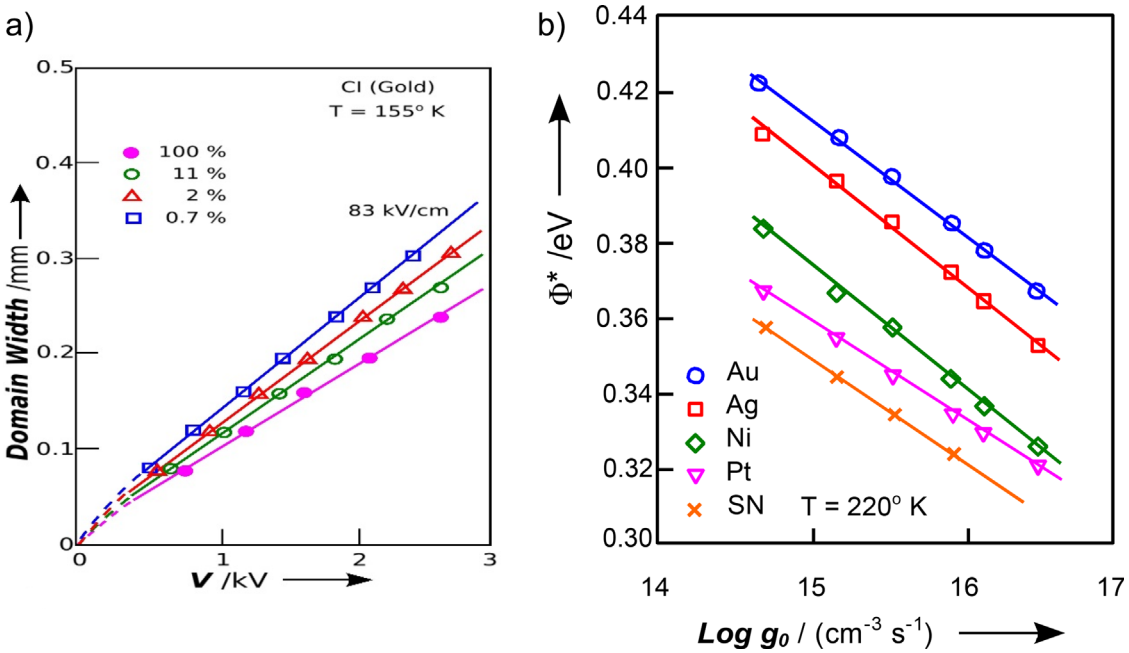

Figure 16 (a) High-field domain width as function of the bias for different light intensities for a gold contact, showing an increasing domain field at decreasing light intensities (given in the figure margin). (b) The work function decreases as function of the optical generation rate, shown for different blocking metal contacts [22, 23]. Reproduced with permission from the Journal of Applied Physics, 107.2, 023701 (2010). Copyright 2010, AIP Publishing LLC.

spread and are constant in the *entire high-field domain that is* ***space-charge free*** and remain in this state as long as the light intensity is not changed. Small (sinusoidal changes) can modulate the position of the quasi-Fermi level and provide an ideal opportunity to measure transition coefficients with the well-known lock-in techniques (LIMA) [24].

3.6.10 First observation of a strong electron quenching signal probably indicating why CdS cannot be doped *p*-type When, with an anode-adjacent domain present, an entire un-doped CdS crystal is exposed to infrared illumination only, then the conductivity maxima at 0.9, 1.3, 1.45 μ appear again, however, interfaced with an extremely sharp and deep electron quenching minimum at 1.05 μ (see Fig. 18).

Such inverted electron quenching with an extremely sharp minimum is remarkable, since, it points to a deep tightly bond level slightly above the middle of the band gap. It is not observed in optical absorption with such a discrete feature probably because of interference with changing fields that broaden the defect level and can only be observed when the high-field domain sweeps the entire crystal free of space charges and hence of interfering electric field fluctuations. It was not observed in the extrinsic range with light induced modulation of absorption spectroscopy (LIMA) [24].

This center could be indicative as an intrinsic center that prevents doping-induced *p*-type, probably due to forced intrinsic compensation.

3.7 Evidence of strong force of the minimum entropy principle Cathode adjacent domains and anode adjacent domains are connected to each other by the same current.

$$j = e\mu_n nF = e\mu_p pF. \tag{7}$$

This is remarkable since the cathode adjacent domain is carried by an electron drift current while the anode adjacent domain is carried by a hole drift current with totally different carrier concentrations and mobilities. Both domains are initiated by a different mechanism of negative differential conductivity for electrons and for holes that is shown in Fig. 8 for electron conductivity in contrast to the picture given in Fig. 19 for hole conductivity.

This is the same current that is saturated and does not change when the domain changes from cathode adjacent to anode adjacent (see arrow in Fig. 12b). This is the strongest evidence that the *minimum entropy principle* determines the current, that now can be expressed by the equation:

$$\frac{dj}{dv} = U, \tag{8}$$

the *minimum entropy equation* that means that the current does not change while the voltage changes in the entire range from cathode- to anode-adjacent domain (Note: we have also called this the life equation since it is responsible for creating all life on earth).

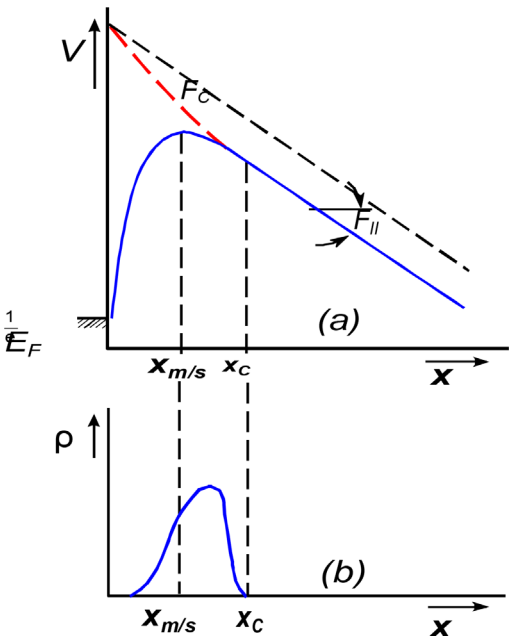

Figure 17 Potential and space charge distribution (schematically) between the Schottky barrier and the high- field domain starting at x_c. For the first part, the potential is determined by the image force, followed by the space charge, determined by depletion of electrons from donors and increases as the distance from the cathode increases, with the potential maximum at the boundary $x_{m/s}$. With further increasing distance from the boundary, the field increases and the field-quenching becomes stronger until the electron density reaches n_c. Then, compensation is completed at x_c, and the high-field domain starts [22, 23]. Reproduced with permission from Physical Review, 179.3, 703 (1969). Copyright 1969, American Physical Society.

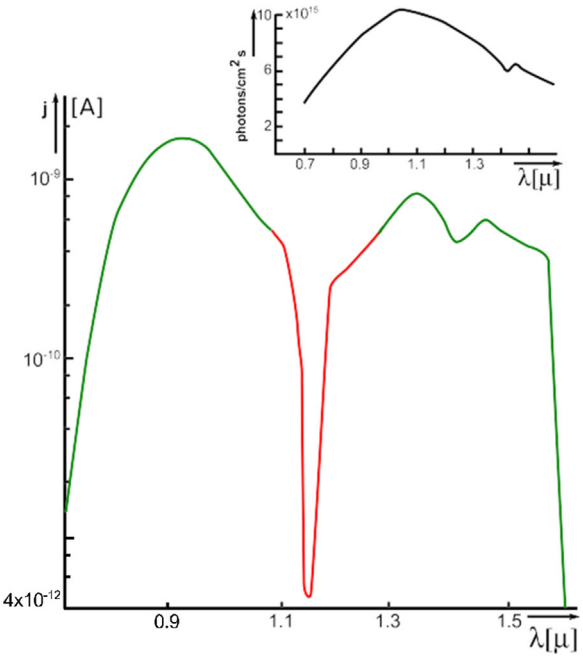

Figure 18 Spectral distribution of the *p*-type photoconductive undoped CdS crystal with gold electrodes while an anode-adjacent high-field domain is present [25]. The deep minimum is shown in red, indicating an electron signal from quenching imbedded in the hole excitation spectrum shown in green [25]. The insert shows the spectral output of the monochromator indicating no such anomaly in the response. Reproduced with permission from Physical Review, 154.3, 757 (1967). Copyright 1967, American Physical Society.

The minimum entropy principle enables us to create a totally new model for the solar cell operation.

4 A new solar cell

4.1 Background In the past, we tried to understand the solar cell by describing it with a diode equation connected to a current generator. There were enough adjustable parameters including a shunt and series resistor and a diode ideality factor to match most measured curves. However, with CIGS solar cells were severe discrepancies between theory and experiment, for example, one expects that the highest band gap material ($CuGaAs_2$) should face the sun, while in fact, cells that have $CuInAs_2$ in front show higher conversion efficiencies. Nobody also could understand why CdS is such a good layer to improve the efficiency while other materials did not.

Therefore, we change our discussion for the *operation* of the cell, including its external circuit to become a more realistic description when exposed to light.

Only when loaded near the maximum power point is the temperature of a solar cell reduced (Fig. 20), while with other loads it returns to the original temperature. This is a convincing experiment [26] to include the external

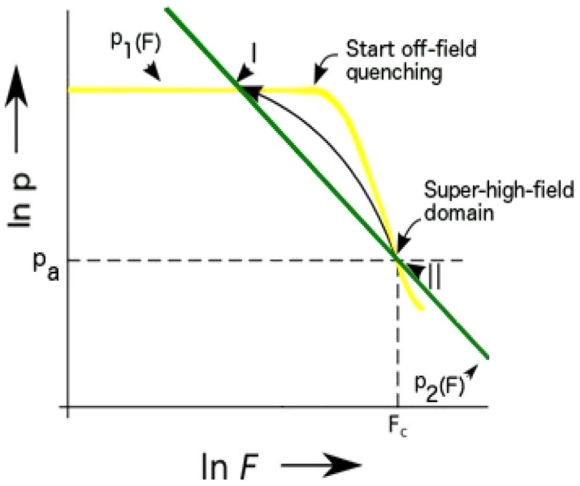

Figure 19 Field-of-direction for holes in p-type CdS that shows negative differential conductivity with steep decrease of $p_1(F)$ and the appearance of the high-field domain when the drift current curve $p_2(F)$ intersects the hole density at the boundary concentation p_a.

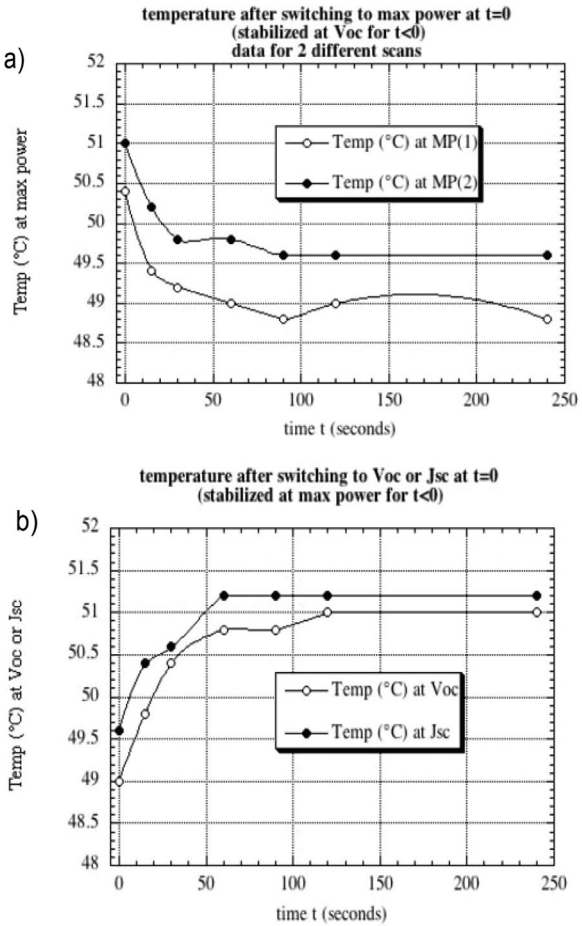

Figure 20 The temperature of a solar cell decreases when power is extracted at maximum power point (a) and it returns to the original temperature when the cell is switched to short circuit or open circuit voltage (b) [26].

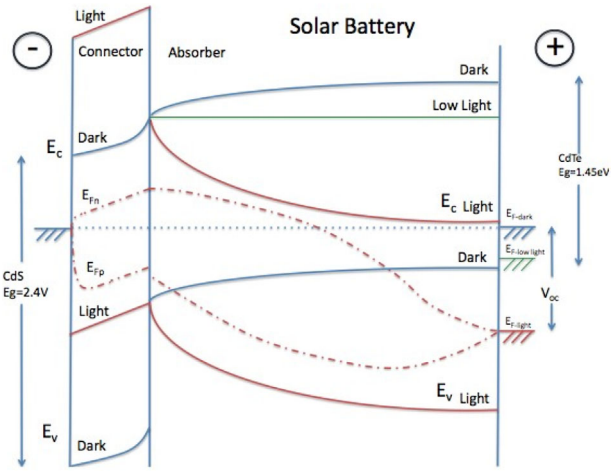

Figure 21 Band model of the CdS/CdTe solar cell under different operating conditions: dark, low light excitation where by extrapolation the bands are flat (shown as green line for the conduction band), and AM1 at maximum power point. It shows the Fermi level in the dark (a straight line between the electrode in thermodynamic equilibrium) and the quasi-Fermi levels for electrons (schematically) and for holes (to indicate the photoelectric current) in steady state. At the left is a thin layer of clean CdS with a junction-adjacent high-field domain [2], that extracts the holes from the CdTe for tunneling into the base electrode at the left of CdS.

circuit and to discuss the operation of the cell near the maximum power point to obtain a meaningful model for the cell.

In the following discussion, we only accept directly measured results, and all basic physics laws, without using tabulated values like electron affinities and work functions. That yields the first to scale model of the CdS/CdTe solar cell.

4.2 The determining influence of the minimum entropy principle The solar cell in operation, close to the maximum power point including the external circuit.

4.3 The new solar cell model The suggested model is shown in Fig. 21 and based on the measured values of a typical CdS/CdTe solar cell [27].

The entire solar cell operation is controlled by *the minimum entropy principle*. The solar energy input provides the energy to excite the holes and shifts the quasi-Fermi levels down from the equilibrium position. It creates the diffusion current (the solar current) form the gradient of E_{Fp} (x) with a minimum close to the center of the CdTe (some losses because of recombination at the electrode of CdTe causes some back diffusion). The amount of the shift of the quasi-Fermi level for holes and hence the voltage at the operational point is determined by the minimum entropy condition. The band distribution is more difficult to understand; it adjusts automatically and is shown only schematically for three cases in Fig. 21.

In the dark, the electron currents connect the conduction bands at the CdS/CdTe interface, since CdS is n-type and the electron current in both materials is dominant and must be continuous at the interface.

In the light, the hole currents in CdTe and CdS are dominant and connects both valence bands because of current continuity. There is a minor jump of both bands at the interface because of the different effective masses of the carriers.

This causes a large shift of the interface dipole moment with changing light intensity, together with the shift of the band edge connection during cell operation. It prevents the back flux of electrons into the CdTe with light; consequently, junction leakage is stopped and the open circuit voltage can approach its theoretical limit approaching the band gap of CdTe when extrapolated to 0 K.

The CdS is passive and therefore the Fermi-level at its electrode remains unchanged during cell operation. For increasing V_{oc} of the solar cell, one needs to dope a thin surface-near layer with shallow donors.

The operation of the CdS is based on a high-field domain. Since the layer is too thin (typically of 400 Å in most deployed CdS/CdTe solar cells) to follow the field

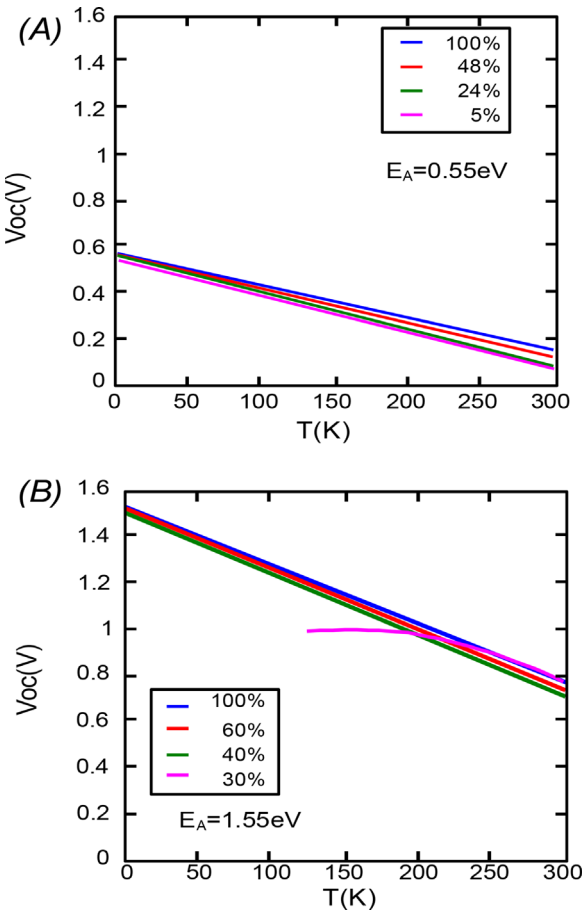

Figure 22 Open circuit voltage (A) of CdTe solar cell as function of temperature for three different light intensities shown in the margin (100% = AM 1.5). (B) Same for the CdS/CdTe solar cell, showing the extrapolation to 0 K at the band gap of CdTe as theoretically expected for a nonleaking junction with a 0.2 V drop below the extrapolated line at 120 K, due to series resistance in the 400 Å thick CdS of the cell [2]. Reproduced with permission from IEEE Proceedings, (2008). Copyright 2008, IEEE.

visually using the Franz–Keldysh effect, we use the knowledge from large crystals and apply it to the situation when CdS is connected to CdTe: At the interface, the field at the junction in CdS is high enough to initiate a high-field domain. In earlier samples, CdS was doped with copper, but in the latest version of the cells that show higher conversion efficiencies (up to 21%) where the CdS is undoped (Note, a recent press release of a CdTe solar cell with 21% efficiency and $V_{oc} = 0.876$ V, $j_{sc} = 30.25$ A cm^{-2}, and FF = 79.4%, however, there is not sufficient other information to draw a band model to this improved cell [28]). With the CdS attached to the junction, the field is sufficient to invert it to become *p*-type. The junction-adjacent domain extends to fill the entire crystal (the Debye length is larger than the crystal thickness).

The CdS extracts all holes that can be supplied by the Richardson–Dushman limit from the CdTe. This limits the hole *drift current* in CdS and stabilizes its operation. In a very thin layer near the base electrode, both quasi-Fermi levels must meet at the Fermi level of the electrode. The holes then tunnel into the electrode.

The current in the domain is given by drift only, and consequently results in a series resistance limitation. For a current of 25 mA cm^{-2}, this causes a drop in V_{oc} by 0.1 V for every 100 Å of CdS thickness. This agrees with the experiment [29] as shown in Fig. 22.

The dramatic increase of the open circuit voltage when the CdS layer is attached is seen by comparison of Fig. 22A and B. The deviation of about 0.2 V below the extrapolated line at 120 K agrees with the theory of a series resistance limitation given above.

5 Summary CdS is a model substance in which its electrical properties can be varied over a very wide range from insulating to highly conductive depending on the excitation by temperature, light or electric field. It is shown that CdS can be made into three thermodynamically stable states, at low fields (the classical CdS) or with a cathode adjacent high field domains that eliminates all space charges within the domain, or with an anode-adjacent domain that turns the CdS *p*-type and is the basis of a new solar cell model.

In the second part, high-field effects are described by introducing the Franz–Keldysh effect that permits direct visualization of the electric field distribution. It is shown that when the conductivity decreases stronger than linearly with the field, high-field domains must occur. When they remain attached to an electrode or a junction, we accepted the name Böer-domain; all other domains should be named Schöll-domains who has analyzed these moving domains. In all domains, the current is constant and the carrier transport is by drift only. The domain field is constant and changes of the applied voltage are absorbed in a change of domain width. The domains can be attached to the cathode, then, the CdS is *n*-type. This domain is stabilized by the limited electron supply from the cathode. Or the domain is attached to the anode and the entire CdS flips to become *p*-type. When attached to a *p*-type solar cell without a *pn*-junction, the leakage through the junction is prevented and a higher V_{oc} results that approaches the band gap of the emitter when extrapolated to 0 K.

Acknowledgements It is with great pleasure that I extend my gratitude to Rommel Noufi who has helped me to clear my mind and develop the new solar cell model, and to Steve Hegedus who supplied some important experimental data. All my gratitude goes to the members of my research team who over the many decades have helped me to understand the physics of CdS, all of them are listed in the many papers I published, but I like to single out Ulrich Kümmel, who discovered the high-field domains, Peter Voss, who brought order into the development of all stationary domains, and Gustavo Dussel who helped me to understand much of the theoretical detail.

References

[1] K. W. Böer and U. Kümmel, Zeitschrift fur Angewandte Physik **12**(6), 241–244 (1960).

[2] K. W. Böer, Annalen der Physik **527**, 378–395 (2015).
[3] K. W. Böer, H. J. Hänsch, and U. Kümmel, Zeitschrift fur Physik **155**, 170–183 (1959).
[4] K. W. Böer, Zeitschrift fur Physik **155**, 184–194 (1959).
[5] K. W. Böer, H. J. Hänsch, and U. Kümmel, Naturwis-senschaften **45**, 460–460 (1958).
[6] K. W. Böer, Phys. Status Solidi B **248**(12), 2775–2785 (2011).
[7] E. Schöll, Nonequilibrium Phase Transitions in Semiconductors: Self-Organization Induced by Generation and Recombination Processes, Springer Series in Synergetics (Springer, Berlin, Heidelberg, 2012).
[8] K. W. Böer, in: Proc. of the International Conferenceon Semiconductor Physics, Prague, 1960, International Conference on the Physics of Semiconductors, (Academic Press, Prague, 1960), chap. Inhomogene FeldUnd Stromverteilungen in Halbleitern Und Isolatoren, pp. 828–832.
[9] K. W. Böer and W. E. Wilhelm, Phys. Status Solidi B Basic Res. **3**, 1704–1717 (1963).
[10] K. W. Böer and H. Vogel, Annalen der Physik **452**, 10–22 (1955).
[11] K. W. Böer, S. Oberländer, and J. Voigt, Zeitschrift Naturforschung Teil A **13**, 544–547 (1958).
[12] K. W. Böer and H. Wantosch, Annalen der Physik Lpz **7.2.7-8**, 406–412 (1959).
[13] K. W. Böer and E. A. Niekisch, Phys. Status Solidi B Basic Res. **1**, 275–305 (1961).
[14] G. A. Dussel and K. W. Böer, Phys. Status Solidi B Basic Res. **39**, 375–389 (1970).
[15] K. W. Böer and P. Voss, Phys. Rev. **171**, 899–903 (1968).
[16] K. W. Böer, Phys. Status Solidi B Basic Res. **249**, 1577–1584 (2012).
[17] K. W. Böer and P. Voss, Phys. Status Solidi B Basic Res. **28**, 355–364 (1968).
[18] K. W. Böer, J. Appl. Phys. **107**(2), 023701 (2010).
[19] R. G. Dhere, Y. Zhang, M. J. Romero, S. E. Asher, M. Young, B. To, R. Noufi, and T. A. Gessert, Investigation of junction properties of cds/cdte solar cells and their correlation to device properties, in: 2008 33rd IEEE Photovoltaic Specialists Conference (PVSC), (US Department of Energy, 2008).
[20] K. W. Böer and W. E. Wilhelm, Phys. Status Solidi B Basic Res. **4**, 237–249 (1964).
[21] R. J. Stirn, K. W. Böer, G. A. Dussel, and P. Voss, Cds-metal workfunctions at higher current-densities, in: Third Photoconductivity Conference (Pergamon Press, Stanford, 1971) pp. 389–394.
[22] R. J. Stirn, K. W. Böer, and G. A. Dussel, Phys. Rev. B **7**, 1433–1443 (1973).
[23] G. A. Dussel, K. W. Böer, and R. J. Stirn, Phys. Rev. B **7**, 1443–1454 (1973).
[24] K. W. Böer, Zeitschrift Naturforschung Teil A **24**, 1306–1310 (1969).
[25] K. W. Böer and J. J. Ward, Phys. Rev. **154**, 757–762 (1967).
[26] K. W. Böer, Phys. Status Solidi A **184**(1), 201–209 (2001).
[27] K. W. Böer, A new solar cell from a clean CdS as connector to a p-type collector without a pn-junction and the minimum entropy principle permits achieving maximum efficiency, J. Appl. Phys. **120**, 165701 (2016).
[28] M. A. Green, K. Emery, Y. Hishikawa, W. Warta, and E. D. Dunlop, Prog. Photovolt. Res. Appl. **23**(7), 805–812 (2015). PIP-15–110.
[29] H. Li, C. S. Jiang, W. K. Metzger, C. K. Shih, and M. Al- Jassim, IEEE J. Photovolt. **400**(1), 395–400 (2015).

